DOI: 10.1093/jnci/djq310
Advance Access publication on August 25, 2010.

ARTICLE

Effect of Multikinase Inhibitors on Caspase-Independent Cell Death and DNA Damage in HER2-Overexpressing Breast Cancer Cells

Samuel Seoane, Juan Carlos Montero, Alberto Ocaña, Atanasio Pandiella

Manuscript received March 24, 2009; revised July 20, 2010; accepted July 26, 2010.

Correspondence to: Atanasio Pandiella, MD, PhD, Instituto de Biología Molecular y Celular del Cáncer-CSIC, Campus Miguel de Unamuno, 37007-Salamanca, Spain (e-mail: atanasio@usal.es).

Background The receptor tyrosine kinase, HER2, is overexpressed in approximately 25% of patients with breast cancer and is implicated in the aggressiveness of cancer. Targeting of HER2 signaling with trastuzumab, a monoclonal antibody that inhibits HER2 activity, has demonstrated clinical benefits.

Methods We investigated whether the antitumor activity of trastuzumab can be potentiated by dasatinib, a small-molecule tyrosine kinase inhibitor, on breast cancer cell lines that overexpress HER2 (BT474 and SKBR3) or have normal HER2 expression (MCF7 and T47D). Functional, biochemical, and gene expression microarray studies were performed to test the effect of trastuzumab, dasatinib, or a combination of trastuzumab and dasatinib on cell proliferation; HER activation; cell cycle; DNA damage; and apoptosis. The effect of drugs on mice (n = 6 per group) bearing xenograft tumors originating from HER2-overexpressing BT474 cells was assessed, and tumors were evaluated for an effect on volume, HER signaling, and DNA damage. All statistical tests were two-sided.

Results Trastuzumab and dasatinib combination showed a synergistic effect on the proliferation of HER2-overexpressing breast cancer cells (combination index = 0.44, 95% confidence interval = 0.30 to 0.58). The drug combination also induced a stronger inhibitory effect on HER2 activation than the individual drugs, decreased the level of proteins involved in DNA damage response, induced DNA double-strand breaks, cell cycle arrest, and caspase-independent apoptosis. Mice (n = 6 per group) bearing xenograft tumors originating from HER2-overexpressing BT474 cells showed statistically significantly reduced tumor volume on day 28 when treated with the drug combination (control vs trastuzumab and dasatinib combination; mean volume = 2.6 vs 0.5 cm^3, difference = 2.1 cm^3, 95% confidence interval = 0.76 to 3.51 cm^3, $P = .01$) and total regression of tumors by day 36 with no later relapse.

Conclusions Results showed that HER2 and dasatinib-sensitive tyrosine kinases act in a synergistic manner to safeguard the breast cancer cells from DNA damage. The therapeutic targeting of multikinase inhibition opens new avenues for the treatment of HER2-positive breast cancer patients.

J Natl Cancer Inst 2010;102:1432–1446

Breast cancer is the most common neoplasia in women. Despite important advances in treatment, metastatic breast cancer is incurable and new treatments to improve patient outcome are needed. Therefore, identification of the key molecular alterations that induce proliferation or drug resistance in breast cancer cells will be helpful in defining potential therapeutic targets.

Tyrosine kinases, either cytosolic (soluble) or transmembrane (membrane-bound), play important roles in animal physiology, and their deregulation has been linked to the development and progression of different types of cancer (1,2). In breast cancer, overexpression of the HER2 (also known as v-erb-b2 erythroblastic leukemia viral oncogene homolog 2), a receptor tyrosine kinase (RTK) (2), occurs in approximately 25% of patients and is associated with shorter survival (3). These findings led to several preclinical studies that confirmed the oncogenic potential of HER2 (4–7) and also led to the development of therapeutic agents targeting HER2 (2). One of these compounds is trastuzumab—a humanized monoclonal antibody that binds to the extracellular domain of HER2 (8,9). In HER2-overexpressing breast tumors, treatment with trastuzumab in combination with other antineoplastic drugs increases patient survival in metastatic and early-stage breast cancer (10,11). Despite the effectiveness of such treatments, a substantial number of HER2-positive patients do not respond to trastuzumab or relapse in a short period of time (12). Therefore, the development of novel therapeutic strategies that are aimed at increasing the efficacy of trastuzumab may help in preventing or delaying relapse in patients with HER2-positive tumors (12). In this context, the combined targeting of HER2 and other tyrosine

kinases presents an interesting strategy because these tyrosine kinases are associated with breast cancer tumorigenesis and are of substantial interest as potential drug targets (12). The insulinlike growth factor 1 receptor (IGF-1R), an RTK, has been shown to increase the growth of breast cancer cells and is also implicated in developing resistance to trastuzumab (13). Indeed, cotargeting of IGF-1R and HER2 offers an important advantage over targeting of the individual RTKs in breast cancer cells (14). The v-kit Hardy-Zuckerman 4 feline sarcoma viral oncogene homolog (c-KIT) RTK is overexpressed in triple-negative breast cancers (those that do not express estrogen receptor, progesterone receptor, and HER2) (15). The activation of two nonreceptor cytosolic tyrosine kinases, c-abl oncogene 1 (ABL1) and c-SRC tyrosine kinase (CSK), is associated with the aggressiveness of breast cancer (16) and proliferation of triple-negative breast cancers (16,17), respectively. Moreover, c-SRC has also been associated with antiestrogen resistance in estrogen receptor–positive breast tumors (18).

Dasatinib, a small-molecule tyrosine kinase inhibitor, has been shown to target the cytosolic c-SRC and ABL1 kinases, as well as the RTKs c-KIT and platelet-derived growth factor receptors alpha and beta (17,19–21). The reported biological activity of dasatinib against triple-negative breast cancer (17,20), together with its favorable antitumoral activity in head and neck cancer when combined with gefitinib (22), led us to explore whether dasatinib could increase the antitumoral effect of trastuzumab on HER2-positive breast cancers.

In this study, we investigated the effects of trastuzumab and dasatinib combination on HER2 activation and HER2-mediated signaling using biochemical and gene expression microarray analyses and determined the effectiveness of the drug combination in preclinical mouse models.

CONTEXT AND CAVEATS

Prior knowledge

Trastuzumab is a humanized monoclonal antibody that binds to and inhibits the activity of HER2, a receptor tyrosine kinase. Although trastuzumab in combination with other anticancer drugs can increase the survival of patients with HER2-positive breast cancer, some do not respond to trastuzumab treatment.

Study design

In vitro and in vivo models of HER2-positive breast cancer were used to investigate if trastuzumab in combination with dasatinib, a tyrosine kinase inhibitor reported to have antigrowth activity in breast cancer cells, showed greater inhibition of breast cancer cell proliferation and tumor development.

Contribution

Trastuzumab and dasatinib combination showed a synergistic effect on the inhibition of HER2-overexpressing breast cancer cell proliferation and a complete regression of tumor xenografts in the in vivo mouse model with no relapse after treatment discontinuation.

Implications

The antitumor activity of trastuzumab can be potentiated by dasatinib in HER2-positive tumors.

Limitations

The efficacy of the drug combination in a mouse model is not indicative of clinical success. In addition, whether an effective dose of the drug combination has an adverse effect in humans is not known.

From the Editors

Materials and Methods

Reagents and Antibodies

Cell culture medium (Dulbecco's modified Eagle medium [DMEM]) and serum (fetal bovine serum [FBS]) were purchased from Invitrogen (Gaithersburg, MD). Protein A-Sepharose was from GE Healthcare Life Sciences (Piscataway, NJ). Immobilon-P membranes were from Millipore Corporation (Bedford, MA). Nitrocellulose membranes were from Bio-Rad Laboratories (Hercules, CA). Trastuzumab and dasatinib were from Roche Diagnostics (Barcelona, Spain) and Bristol-Myers Squibb (Princeton, NJ), respectively. Other generic chemicals were purchased from Sigma-Aldrich (St Louis, MO), Roche Biochemicals (Hoffmann, Germany), or Merck (Darmstadt, Germany). The caspase inhibitors (Z-IETD-FMK, Z-LEHD-FMK, and Z-VAD-FMK) were obtained from BD Biosciences (San Jose, CA).

The following antibodies were purchased from Santa Cruz Biotechnology (Santa Cruz, CA)—rabbit polyclonal anti-HER3 antibody (raised against the carboxyl [C] terminus of human HER3; 1 μg/mg of protein lysate for immunoprecipitation, 0.1 μg/dot for dot blot, and 1:5000 dilution for immunoblot studies); mouse monoclonal IgG2a anti-HER4 (raised against an epitope mapping between amino acids 1280–1308 at the C terminus of human HER4; 1 μg/mg of protein lysate for immunoprecipitation, 0.1 μg/dot for dot blot, and 1:5000 dilution for immunoblot studies); mouse monoclonal IgG2b anti-phosphotyrosine (clone PY99, 1:10 000 dilution); rabbit polyclonal IgG anti–myeloid cell leukemia sequence 1 (MCL1) (raised against an epitope mapping within an internal region of human MCL1; 1:2000 dilution); rabbit polyclonal anti–baculoviral IAP repeat-containing 2 protein (BIRC2, also known as c-IAP-1 inhibitor of apoptosis protein 1) (raised against an epitope corresponding to amino acids 111–193 mapping within an internal region of human BIRC2; 1:2000 dilution); mouse monoclonal anti–glyceraldehyde-3-phosphate dehydrogenase (1:10 000 dilution); rabbit polyclonal anti–nuclear apoptosis–inducing factor 1 (NAIF1, also known as AIF-1) (raised against an epitope corresponding to amino acids 1–300 mapping at the amino [N] terminus of human NAIF1; 1:2000 dilution); rabbit polyclonal anti-SRC antibody (raised against the N terminus of human SRC; 1:1000 dilution); rabbit polyclonal anti–protein tyrosine kinase-2 (PTK2, also known as focal adhesion kinase [FAK]) (raised against the C terminus of human FAK; 1:1000 dilution); mouse monoclonal anti–SRC homology 2 domain–containing transforming protein 1 (SHC1) (raised against an epitope corresponding to amino acids 366–473 of human SHC1; 1:5000 dilution); goat polyclonal anti-AKT1 (raised against the C terminus of human AKT1; 1:1000 dilution); rabbit polyclonal anti–mitogen-activated protein kinase 1 (MAPK1, also known as ERK1) (raised against an epitope mapping to the C terminus of ERK2 of rat origin, cross

reacts with both human ERK1 and ERK2; 1:10 000 dilution); mouse monoclonal IgG2a anti–cyclin-dependent kinase-2 (CDK2) (raised against human recombinant CDK2; 1:1000 dilution); rabbit polyclonal anti-cyclin E1 (CCNE1) (raised against the C terminus of human cyclin E1, also recognizes cyclin E2 [CCNE2]; 1:1000 dilution); rabbit polyclonal anti-cyclin B1 (CCNB1) (raised against an epitope corresponding to amino acids 1–300 of human cyclin B1; 1:1000 dilution); rabbit polyclonal anti–cyclin-dependent kinase inhibitor 1A (CDKN1A, also known as p21) (raised against the C terminus of human p21; 1:5000 dilution); rabbit polyclonal anti–cyclin-dependent kinase inhibitor 1B (CDKN1B, also known as p27) (raised against the C terminus of human p27; 1:5000 dilution); rabbit polyclonal anti–excision repair cross-complementing rodent repair deficiency, complementation group 4 (ERCC4, also known as RAD1) (raised against an epitope corresponding to amino acids 1–282 of human RAD1; 1:1000 dilution); rabbit polyclonal anti-RAD51 (raised against an epitope corresponding to amino acids 1–92 of human RAD51; 1:1000 dilution); mouse monoclonal anti-RAD54B (clone 19-K2, raised against recombinant RAD54B; 1:1000 dilution); rabbit polyclonal anti-RAD50 (raised against an epitope corresponding to amino acids 1013–1312 mapping to the C terminus of human RAD50; 1:1000 dilution); and goat polyclonal anti–meiotic recombination 11 homolog A (MRE11A) (raised against the C terminus of human MRE11A; 1:5000 dilution).

The mouse monoclonal anti-HER2 antibody (clone Ab-3, recognizes an epitope corresponding to amino acids 1242–1255 at the C terminus of human HER2; 1 μg/mg of protein lysate for immunoprecipitation, 0.1 μg/dot for dot blot, and 1:10 000 dilution for immunoblotting) was purchased from Calbiochem (La Jolla, CA); cetuximab, the anti–epidermal growth factor receptor (EGFR) (also known as HER1) antibody (1 μg/mg of protein lysate for immunoprecipitation and 0.1 μg/dot for dot blot), was purchased from Merck (Madrid, Spain). A polyclonal anti-EGFR antibody (raised against the amino acids 909–1210 of the C terminus of human EGFR, dilution 1:5000 for immunoblotting) was raised in our laboratory (23).

The following rabbit polyclonal antibodies were purchased from Cell Signalling Technology (Beverly, MA)—anti-phosphorylated (Tyr1248) HER2 (1:1000 dilution); anti–phosphorylated (Tyr416) SRC (1:1000 dilution); anti–phosphorylated (Tyr421/Ser424) ribosomal protein S6 kinase, 70 kDa, polypeptide 2 (RPS6KB2, also known as p70S6K) (1:5000 dilution); anti–phosphorylated (Ser136) BCL2-associated agonist of cell death (BAD) (1:1000 dilution); and anti–phosphorylated (Ser139) H2A histone family, member X (H2AFX, also known as H2AX, and its phosphorylated form at this site is known as γH2AX) (1:1000 dilution). The rabbit monoclonal anti-BAD antibody (clone 11E3; 1:1000 dilution) and the mouse monoclonal anti–phosphorylated (Ser1981) ataxia telangiectasia mutated (clone 10H11.E12; 1:1000 dilution) were also purchased from Cell Signalling Technology.

The following antibodies were purchased from BD Biosciences—the mouse monoclonal anti-caspase-3 (CASP3) (clone 19, raised against amino acids 1–219 of human caspase 3; 1:2000 dilution); mouse monoclonal anti-caspase-8 (CASP8) (clone 3-1-9, raised against full-length recombinant human caspase 8; 1:1000 dilution); mouse monoclonal anti-caspase-9 (CASP9) (clone 2-22, raised against amino acids 1–134 of human caspase-9; 1:1000 dilution); mouse monoclonal anti–B-cell CLL/lymphoma 2 (BCL2) (clone 6C8, raised against human recombinant BCL2; 1:2000 dilution); rabbit polyclonal anti–BCL2-like 1 (BCL2L1, also known as BCL-X) (raised against amino acids 18–233 of human BCL2L1; 1:5000 dilution); and mouse monoclonal anti–phosphotyrosine-horseradish peroxidase (HRP) (clone PY20; 1:1000 dilution).

The cyanine 3 (Cy-3)–conjugated secondary antibodies were from Jackson ImmunoResearch Laboratories, Inc (West Grove, PA); Alexa 488-conjugated antibody was from Invitrogen; HRP conjugates of anti-rabbit and anti-mouse IgG were from Bio-Rad Laboratories; rabbit polyclonal anti-calnexin antibody was from Stressgen Biotechnologies Corporation (Victoria, Canada); and anti–phosphorylated human AKT (Serine 473) antibody was raised in our laboratory against the amino acid sequence RPHFPQFpS473YSAS (p = phosphorylated).

Cell Culture

Four breast cancer cell lines—BT474, SKBR3, MCF7, and T47D—were grown in DMEM supplemented with 10% FBS, 100 mU/mL penicillin (Invitrogen), 100 μg/mL streptomycin (Invitrogen), and 2 mM L-glutamine (Invitrogen) in a 5% CO_2 atmosphere at 37°C. The cell lines were obtained from the American Type Culture Collection Cell Biology Collection (Manassas, VA). The BT474 and SKBR3 cell lines overexpress HER2 receptor, whereas MCF7 and T47D cell lines have normal HER2 expression (24). The level of HER2 proteins in these cell lines was verified by immunoblotting (Supplementary Figure 1, available online).

For three-dimensional cell culture, 12-mm coverslips were coated with 60 μL of ice-cold Matrigel (BD Biosciences) and incubated at 37°C for 20 minutes to allow the Matrigel to solidify. Cells were treated for 5 minutes with 0.25% trypsin–EDTA solution (2.5 g/L of trypsin, 0.38 g/L of EDTA) (Invitrogen). A single-cell suspension containing 5×10^3 cells per 100 μL volume of medium, supplemented with 2% (vol/vol) of Matrigel, was carefully placed on top of the solidified Matrigel. Incubation was carried out at 37°C for 30 minutes to allow the cells to attach to the Matrigel. The coverslips were then placed in six-well plates, 500 μL of medium was added per well, and the cells were cultured for 10 days. Cells were then treated with different drugs (10 nM trastuzumab, 1 μM dasatinib, or a combination of 10 nM trastuzumab and 1 μM dasatinib) for 1 week. Selection of the combination dose of trastuzumab was based on previously reported data (14). Phase contrast photographs of cells as monolayers, or in three-dimensional cultures, were taken with a Nikon Eclipse Ti-S inverted microscope (Izasa, Barcelona, Spain). The microscope was equipped with a ProgRes C3 camera and the ProgRess CapturePro 2.7 software, purchased from Jenoptik (Jena, Germany). Quantitation of the sphere diameters was performed manually by tracing a straight line across the diameter of the sphere and scoring its value as arbitrary length units. Two hundred spheres were scored for each condition, and the mean and 95% confidence interval (CI) values were calculated.

Immunoprecipitation and Immunoblotting

BT474, SKBR3, MCF7, and T47D cells were grown in DMEM with 10% of FBS and at 80% confluence (2 days later) were treated with drugs (10 nM trastuzumab, 1 μM dasatinib, or a combination

of 10 nM trastuzumab and 1 μM dasatinib) for 48 hours. Cells were washed with phosphate-buffered saline (PBS) (137 mM NaCl, 2.7 mM KCl, 8 mM Na_2HPO_4, 1.5 mM KH_2PO_4) and lysed in ice-cold lysis buffer (20 mM Tris–HCl [pH 7.0], 140 mM NaCl, 50 mM EDTA, 10% glycerol, 1% Nonidet P-40, 1 μM pepstatin, 1 μg/mL aprotinin, 1 μg/mL leupeptin, 1 mM phenylmethyl sulfonyl fluoride, 1 mM sodium orthovanadate). Lysates were centrifuged at 10 000*g* at 4°C for 10 minutes, and supernatants were treated with the corresponding antibody and protein A-Sepharose. Immunoprecipitations were performed at 4°C for at least 2 hours; immune complexes were recovered by a short centrifugation at 10 000*g* for 15 seconds, followed by three washes with 1 mL cold lysis buffer. Samples were then boiled in electrophoresis sample buffer and placed on 6%–15% sodium dodecyl sulfate–polyacrylamide gel electrophoresis (SDS-PAGE) gels, depending on the molecular weight of the proteins to be analyzed. Immunoblotting was performed as previously described (25). Briefly, after electrophoresis, proteins in gels were transferred to polyvinylidene difluoride membranes (Millipore Corporation). Membranes were blocked in Tris-buffered saline with Tween (TBST) (100 mM Tris [pH 7.5], 150 mM NaCl, 0.05% Tween 20) containing 1% of bovine serum albumin for 1 hour and then incubated with the corresponding antibody for 2–16 hours. After washing with TBST, membranes were incubated with HRP-conjugated anti-mouse or anti-rabbit secondary antibodies (1:10 000 dilution) for 30 minutes and bands were visualized by using ECL Plus Western Blotting Detection System (GE Healthcare, Buckinghamshire, United Kingdom).

Dot Blots and Antibody Arrays

For dot blots, each antibody (0.1 μg) was adsorbed onto a nitrocellulose membrane. The membrane was dried at room temperature for 30 minutes and then blocked for 2 hours in TBST containing 5% bovine serum albumin. The membranes were then incubated with 1 mg of protein lysates overnight at 4°C. The membranes were washed in TBST three times and incubated for 2 hours with the anti–phosphotyrosine-HRP antibody (1:5000 dilution). After three washes of 10 minutes each in TBST, membranes were incubated with the ECL Plus Western Blotting Detection System. The BT474 cell lysates were used as the positive control, as they contain high levels of resting tyrosine phosphorylation of several cellular proteins (26).

To perform the dot blot analyses with commercial arrays, we used the human phospho-RTK array kit (R&D Systems, Abingdon, United Kingdom) and followed the manufacturer's instructions.

Cell Surface Biotinylation and Cell Fractionation

For cell surface biotinylation, BT474 cells (2×10^6 cells per 100-mm dishes) were cultured in DMEM supplemented with 10% FBS, until the cells reached 80% confluence. Cells were then treated with different drugs (10 nM trastuzumab, 1 μM dasatinib, or a combination of 10 nM trastuzumab and 1 μM dasatinib) for 48 hours. Cell monolayers were washed twice with ice-cold Krebs–Ringer–HEPES (KRH) (129 mM NaCl, 5 mM $NaHCO_3$, 4.8 mM KCl, 1.2 mM KH_2PO_4, 1 mM $CaCl_2$, 1.2 mM $MgCl_2$, 2.8 mM glucose, 10 mM HEPES free acid [pH 7.4]) and then incubated with *N*-hydroxysulfosuccinimide-LC-biotin (Thermo Scientific Pierce Protein Research Products, Rockford, IL) (100 μg/mL) for 2 hours at 4°C. Cells were washed again with KRH and then incubated with KRH containing 10 mM glycine for 15 minutes at 4°C. Cell monolayers were washed and lysed, and the lysates were precipitated with anti-HER2 antibodies. Samples were subjected to 8% SDS-PAGE gels and analyzed by immunoblotting using streptavidin–HRP secondary antibody (Sigma-Aldrich).

For cell fractionation experiments, BT474 cells were cultured as above in 100-mm dishes, washed with PBS, incubated in cell dissociation buffer (0.25 M sucrose, 1 mM EDTA, 1 mM phenylmethyl sulfonyl fluoride, and 10 mM Tris–HCl [pH 7.0]) for 10 minutes at 37°C. The cell suspension was homogenized on ice with a tight-fitting Dounce homogenizer (50 strokes) (Kontes Glass Company, Vineland, NJ). This homogenate was centrifuged at 4000*g* for 10 minutes. The resulting pellet was rehomogenized (50 strokes) and centrifuged at the same speed. The supernatants from these two centrifugation steps were pooled and centrifuged at 30 000*g* for 30 minutes. The supernatant was taken as the cytosolic fraction and the pellet as the microsomal fraction.

MTT metabolization, Cell Cycle, and Apoptosis Assays

Cell proliferation experiments were carried out using 3-(4,5-dimethylthiazol-2-yl)-2,5-diphenyltetrazolium bromide (MTT) assays, where MTT is reduced to purple formazan by the mitochondria of living cells. Increase in cell number is detected by augmented MTT metabolization, and decrease in cell number is reflected by decrease in MTT metabolization. BT474, SKBR3, MCF7, and T47D cells were plated at a density of 1×10^4 cells per well in 24-well plates and cultured overnight in DMEM supplemented with 10% FBS. Each well was replaced with 250 μL of fresh medium containing MTT (0.5 μg/μL) and incubated for 1 hour. The medium was then removed and 500 μL of dimethyl sulfoxide was added to each well. The plate was agitated in the dark for 5 minutes to dissolve the MTT-formazan crystals. The absorbance of the samples was recorded at 570 nm in a multiwell plate reader (Tecan ULTRA Evolution, Männedorf, Switzerland). The first measurement was performed 24 hours after the cells were plated and before the addition of the drugs. This value was considered to be the baseline value. Then, drugs (10 nM trastuzumab, 1 μM dasatinib, or a combination of 10 nM trastuzumab and 1 μM dasatinib) were added to the respective wells, and MTT measurements were performed at 2, 3, and 5 days after treatment. In case of dasatinib, we used three doses (0.1, 1, and 10 μM) to plot the dose–response curves in all four breast cancer cell lines. The selected doses were one order of magnitude above (10 μM) and below (0.1 μM) the dose of dasatinib (1 μM) previously found to be effective in triple–negative breast cancer cell lines (17) and also spanned the dose range that previously showed inhibition of proliferation in a large panel of cancer cell lines (20). Results were plotted as the mean (95% CI) values of quadruplicates from a representative experiment that was repeated at least two independent times.

For cell cycle analyses, BT474 cells were cultured in 100-mm culture dishes, grown to 50%–70% confluence, and treated with drugs (10 nM trastuzumab in PBS, 1 μM dasatinib in dimethyl sulfoxide [final dimethyl sulfoxide concentration 1:1000], or a combination of 10 nM trastuzumab and 1 μM dasatinib) for

48 hours. Cell monolayers were then incubated in trypsin–EDTA and resuspended in 1 mL of PBS. After three washes with PBS, the cell pellets were resuspended in 70% ethanol and incubated for 30 minutes at 4°C. Cells were centrifuged at 135*g*, and cell pellets were treated with 1 mL of propidium iodide (PI) staining solution (PBS containing 50 μg/mL of PI, 0.5% Tween 20, 0.1 μg/mL RNase A) (Sigma-Aldrich). DNA content and cell cycle analyses were performed by using a FACScalibur flow cytometer and the CellQuest software (BD Biosciences).

For apoptosis analyses, BT474 cell monolayers were incubated in trypsin–EDTA, washed twice with cold PBS, and then resuspended in binding buffer (10 mM HEPES free acid [pH 7.4], 140 mM NaCl, 2.5 mM $CaCl_2$) at a concentration of 1×10^6 cells per mL. A total of 1×10^5 cells were incubated for 15 minutes in the dark with Annexin V-fluorescein isothiocyanate (BD Biosciences) and PI staining solution (5 μL Annexin V-fluorescein isothiocyanate, 10 μL of PI [5 μL/mL final concentration], 400 μL binding buffer).

The loss of mitochondrial membrane potential, which is indicative of apoptosis, was evaluated by measuring the fluorescence of tetramethylrhodamine ethyl ester (TMRE) dye (Invitrogen). TMRE is a cell-permeant fluorescent dye sequestered by the active mitochondria and shows reduced staining when mitochondria are damaged. Briefly, 2.5×10^5 BT474 cells were plated in 60-mm culture dishes, and after 48 hours of treatment with drugs (10 nM trastuzumab, 1 μM dasatinib, or a combination of 10 nM trastuzumab and 1 μM dasatinib), TMRE (1 μM) was added to the plate for 30 minutes. Cells were treated with trypsin–EDTA solution and resuspended in 500 μL of PBS before quantitation of fluorescence (excitation 488 nm, emission 570 nm) on FACScalibur flow cytometer. The data presented as a histogram differentiated between cells that preserved TMRE fluorescence (intact mitochondria or alive cells) and cells that lost TMRE fluorescence (damaged mitochondria or apoptotic cells). The percentage of cells that lost the staining is represented as the mean (95% CI) of three independent experiments.

To determine whether the combination of trastuzumab and dasatinib was synergistic, additive, or antagonist, we used the CalcuSyn v2.0 software programme (Biosoft, Ferguson, MO). This program allows the calculation of the combination index based on the algorithm of Chou and Talalay (27). Combination index values less than 1 indicate synergism, values equal to 1 indicate an additive effect, whereas values greater than 1 indicate antagonism. Combination index values from three independent experiments were generated. Results were plotted as the mean (95% CI) values of duplicates from two independent experiments.

Cell Surface Immunofluorescence

BT474 cells were grown in DMEM with 10% of FBS, and at 80% confluence were treated with trypsin–EDTA and seeded on glass coverslips. When cells were 30% confluent on the coverslips, they were incubated with anti-HER2 antibody for 2 hours at 4°C, washed with PBS, and fixed in 2% paraformaldehyde for 30 minutes at room temperature. Cells were washed twice in PBS and thrice in PBS with 0.2% bovine serum albumin for 10 minutes each. The cells were then incubated with Cy-3-conjugated secondary antibodies (1:1000) for 30 minutes and washed thrice in PBS with 0.2% bovine serum albumin. Cells were counterstained with 4′,6-diamidino-2-phenylindole to detect cell nuclei, and then the coverslips were mounted onto microscope slides. Samples were analyzed by regular epifluorescence microscopy or by confocal immunofluorescence microscopy using a Zeiss LSM 510 Confocal Microscope (Carl Zeiss Microimaging, Barcelona, Spain). To avoid interference between fluorescence signals, images were captured using multitracking mode (excitation 480 nm, emission 570 nm). The intensity maps, generated by quantification of the intensity of each pixel, were obtained using the LSM 510 software as previously described (23). The software uses a color-based scale to represent the intensities of each pixel (from blue color that represents the lower intensities to red color that represents the higher intensities).

Microarray Analysis of mRNA

BT474 cells were grown in DMEM with 10% of FBS, and when 80% confluent, cells were treated with drugs (10 nM trastuzumab, 1 μM dasatinib, or a combination of 10 nM trastuzumab and 1 μM dasatinib) for 48 hours. Total RNA was extracted and purified using the PureLink Micro-to-Midi kit (Invitrogen). Double-stranded cDNA and biotinylated cRNA were synthesized using a T7-polyT primer and the BioArray RNA labeling kit (Enzo Life Sciences, Farmingdale, NY), respectively. The labeled RNA was fragmented and hybridized to human oligonucleotide arrays (HU-133 Plus 2.0) (Affymetrix, Santa Clara, CA) according to the manufacturer's instructions. For the microarray data analysis, Affymetrix CEL files from each of the two microarray hybridization experiments for the four conditions (untreated control, 10 nM trastuzumab, 1 μM dasatinib, and a combination of 10 nM trastuzumab and 1 μM dasatinib) were imported into the dChip software (Dana Farber Cancer Institute, Boston, MA) (28). Normalization of all arrays was done against the array with median overall intensity. Genes with low expression values (<100 arbitrary units) were considered as "absent" and were discarded from the analysis. Genes with expression values greater than 100 were analyzed for differential expression in pairs of treatment conditions (control vs trastuzumab, control vs dasatinib, control vs trastuzumab and dasatinib combination, trastuzumab vs dasatinib, trastuzumab vs trastuzumab and dasatinib combination, dasatinib vs trastuzumab and dasatinib combination). The genes with greater than or equal to twofold change in expression ($P < .05$, Student t test two-sided) were studied using the Ingenuity Pathway Analysis software (IPA 8.6; Ingenuity Systems Inc., Redwood City, CA). This software allows functional grouping of genes according to their participation in cellular processes, such as cell cycle regulation, DNA damage, adhesion, signaling, and cell metabolism, among many others.

Evaluation of DNA Fragmentation by Comet Assay

Neutral comet assays that detect DNA single- and double-strand breaks (DSBs) were performed using a protocol for the single-cell gel electrophoresis assay (29). Comet assays are based on the staining of individual cellular nuclei in cells exposed to an electrophoretic field. If the nuclear DNA is intact, the image obtained is circular. If nuclear DNA suffers breaks, upon exposure to the electric field the fragmented DNA offers a characteristic "comet" appearance of the nuclei, with a head and a trailing tail. The tail length is proportional to the DNA damage. For this assay, BT474

cells were treated with drugs (10 nM trastuzumab, 1 μM dasatinib, or a combination of 10 nM trastuzumab and 1 μM dasatinib) for 48 hours. After treatment, cells were suspended in 1 mL of 1% low–melting point agarose (Pronadisa, Madrid, Spain). Microscope slides were coated with 100 μL of agarose containing cells and incubated at 4°C in the dark to allow the agarose to solidify. The slides were placed inside a 100-mm plate and submerged in lysis buffer (2.5 M NaCl, 100 mM EDTA, 10 mM Tris–HCl [pH 10], then 0.01 (vol/vol) Triton X-100 was added overnight). After overnight lysis of the agarose-embedded cells, the slides were subjected to electrophoresis in Tris–borate–EDTA (TBE) buffer (100 mM Tris, 100 mM boric acid, 10 mM EDTA, pH 10) for 30 minutes at 1.5 V/cm. The slides were stained with 80 μL ethidium bromide (2 μg/mL) for 5 minutes and then dipped in chilled distilled water to remove the excess stain. Finally, the slides were dried and DNA was observed at ×40 objective using an Axioplan 2 fluorescence microscope (Carl Zeiss Microimaging) equipped with a charge-coupled device camera. Fifty cells by condition (control, 10 nM trastuzumab, 1 μM dasatinib, combination of 10 nM trastuzumab and 1 μM dasatinib) were examined. Comet lengths (head plus tail, in micrometers) were measured with the OpenLab 5.0 (Florence, Italy) software, used to also acquire microphotographs.

Xenograft Studies

Female BALB/c nude mice, 7 weeks old, were obtained from Charles River Laboratories (Wilmington, MA). For efficient tumor growth, the mice (n = 6 per group) were implanted subcutaneously with 1.7 mg, 60-day release, 17β-estradiol pellets (Innovative Research, Sarasota, FL). One week later, 1×10^7 BT474 cells in 200 μL of DMEM and 200 μL of Matrigel were injected into the mammary fat pads of mice. Two weeks after the injection, mice (n = 6 per group) were randomly assigned into four groups (with equal average tumor volumes before initiation of treatments)—vehicle, trastuzumab, dasatinib, and drug combination (trastuzumab and dasatinib combination). The mice were treated twice per week with abdominal injection of 600 μg trastuzumab in PBS and/or once daily orally with 10 mg/kg dasatinib dissolved in 25 mM tartaric acid. Tumor diameters were serially measured with a digital caliper (Proinsa, Vitoria, Spain) every 4 days, and tumor volumes were calculated using the following formula: $V = (L \times W^2)/2$, where V = volume (cubic millimeters), L = length (millimeters), and W = width (millimeters). For biochemical analyses, tumors were resected on day 28 after initiation of treatments. The mice were killed by CO_2 inhalation, and the tumors were resected and frozen in liquid nitrogen. Mice were handled at the institute's (Servicio de Experimentación Animal, Salamanca, Spain) animal facility, and all treatments were in accordance with the legal and institutional guidelines.

Statistical Analysis

Comparison of continuous variables between two groups for in vitro assays and xenograft tumor model experiments was done using a two-sided Student t test. At least two independent experiments were performed for both in vitro and in vivo studies. The differences between different drug treatment groups were considered to be statistically significant when the P values were less than .05. Means and 95% confidence intervals are reported, unless indicated otherwise. All data were analyzed using the statistical software SPSS 15.0 (SPSS, Inc, Chicago, IL).

Results

Effect of Trastuzumab and Dasatinib Combination on the Proliferation of Breast Cancer Cells

To investigate a potential synergistic effect of trastuzumab and dasatinib combination on the growth of breast cancer cells, we used two cell lines (BT474 and SKBR3) that represent in vitro models of HER2 receptor overexpression and activation (23), as well as two cell lines (MCF7 and T47D) with normal HER2 receptor expression (27). We first checked the overexpressed and phosphorylated HER2 protein levels (Supplementary Figure 1, A and B, respectively, available online) in BT474 and SKBR3 cells. To determine the right doses of dasatinib for use in combination with trastuzumab, we tested the sensitivity of the breast cancer cell lines (BT474, SKBR3, MCF7, and T47D) to dasatinib (Supplementary Figure 1, C, available online). The MTT metabolization results indicated that 1 μM and lower concentrations of dasatinib could be used for experiments in combination with trastuzumab, as these doses inhibited cell proliferation and were within the range of clinically achievable concentrations (17,20). Previous studies indicated that 10 nM of trastuzumab represents an optimal concentration for drug combination studies (14).

We next investigated the effect of trastuzumab and dasatinib combination on the growth of breast cancer cells (Figure 1, A). In BT474 and SKBR3 cell lines, the drug combination had a greater inhibitory effect on cell growth compared with treatments with single-agent trastuzumab or dasatinib (BT474: trastuzumab vs drug combination, mean growth = 93% vs 36%, difference = 57%, 95% CI = 42.2% to 71.7%, $P < .001$; dasatinib vs drug combination, mean growth = 73.5% vs 36%, difference = 37.5%, 95% CI = 24.9% to 50%, $P < .002$; SKBR3: trastuzumab vs drug combination, mean growth = 94.2% vs 37%, difference = 57.2%, 95% CI = 50.8% to 63.6%, $P < .001$; dasatinib vs drug combination, mean growth = 66.7% vs 37%, difference = 29.7%, 95% CI = 21.8% to 37.6%, $P < .001$) (Figure 1, A). In contrast, in MCF7 and T47D cell lines, the drug combination did not show a greater inhibitory effect compared with dasatinib alone.

In BT474 cells, dasatinib enhanced the inhibitory effect of trastuzumab on cell growth in a dose-responsive manner (Figure 1, B). To analyze whether the combined effect was synergistic, we used the Chou–Talalay algorithm for combination index analysis (27) and found that low doses of dasatinib showed an additive effect with trastuzumab (0.1 μM dasatinib in combination with trastuzumab: combination index = 1.16, 95% CI = 1.05 to 1.27; 0.25 μM dasatinib in combination with trastuzumab: combination index = 1.11, 95% CI = 1.03 to 1.19; 0.5 μM dasatinib in combination with trastuzumab: combination index = 1.05, 95% CI = 0.96 to 1.15), whereas 1 μM of dasatinib in combination with trastuzumab showed a strong synergistic effect (combination index = 0.44, 95% CI = 0.30 to 0.58) (Figure 1, C).

Trastuzumab and dasatinib combination also affected the morphology of BT474 cells. In culture dishes, BT474 cells grow as monolayers and form island-like clusters. The drug combination

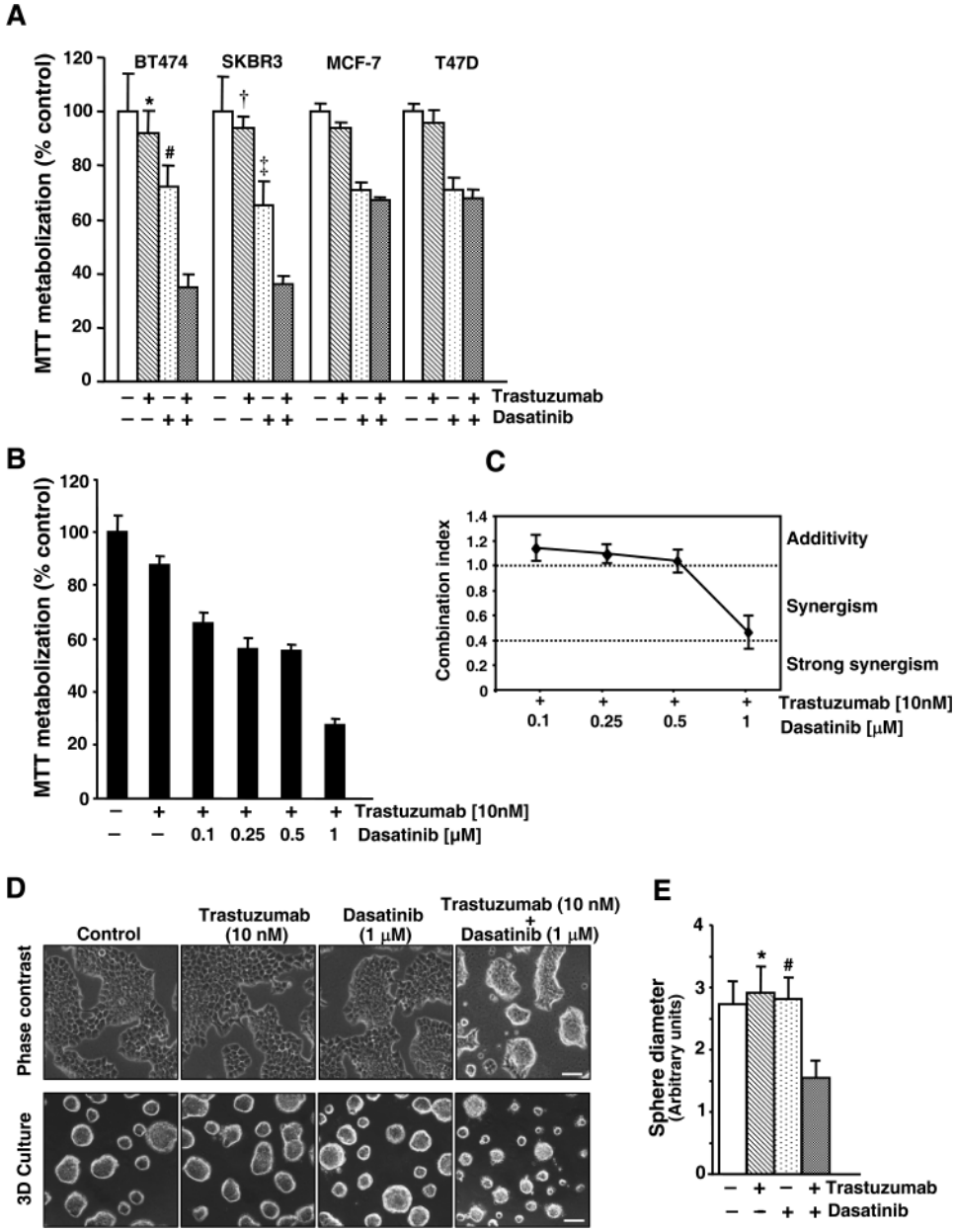

Figure 1. Effect of trastuzumab and dasatinib combination on the proliferation of breast cancer cells. **A**) BT474, SKBR3, MCF7, and T47D cells were cultured in the presence of trastuzumab (10 nM) or dasatinib (1 μM) or a combination of both drugs, and 3-(4,5-dimethylthiazol-2-yl)-2,5-diphenyltetrazolium bromide (MTT) metabolization was measured. Briefly, cells were treated with the indicated drugs, and after 3 days, MTT was added. Absorbance was measured at 570 nm. The mean absorbance values of untreated samples from each cell line were taken as 100%. Absorbance values of the cells treated with different drugs are plotted as percentages with respect to the mean value of the untreated samples. Means and 95% confidence intervals of an experiment representative of three independent experiments performed in quadruplicate are shown. In BT474: $*P < .001$, trastuzumab vs drug combination; $\#P = .002$, dasatinib vs drug combination. In SKBR3: $\dagger P < .001$, trastuzumab vs drug combination; $\ddagger P < .001$, dasatinib vs drug combination. Student *t* test (two-sided) was used to compare means between groups and to calculate *P* values. **B**) Dose–response analysis of dasatinib on the proliferation of BT474 cells treated with trastuzumab. Cells were treated with trastuzumab (10 nM) in combination with different doses (0.1, 0.25, 0.5, or 1 μM) of dasatinib, and MTT metabolization was measured after 3 days. Control cells were untreated. The results show the means and 95% confidence intervals of an experiment, performed two independent times in quadruplicate. **C**) The combination index values were calculated using the CalcuSyn software. The graph shows the means and 95% confidence intervals of two independent experiments performed in triplicate. **D)** Effect of trastuzumab, dasatinib, and the drug combination on the morphology of BT474 cells grown as monolayers (**top panels**) or as three-dimensional (3D) cultures (**bottom panels**). To assess the effect of different drugs on the morphology of BT474 cell monolayers (**top panels**), 5×10^5 cells were plated in 100-mm dishes, allowed to adhere for 24 hours, then trastuzumab (10 nM), dasatinib (1 μM), or a combination of both drugs were added. The images were taken after 48 hours. To assess the effect of different drugs on BT474 cells grown as 3D cultures, 5×10^3 cells were grown in semisolid media for 10 days and then treated with trastuzumab (10 nM), dasatinib (1 μM), or a combination of both drugs, for an additional 7 days (**bottom panels**). All images were taken at ×25 magnification. Scale bar = 50 μm. **E**) Bar graph representation of the sphere diameters in 3D cultures. BT474 cells grown as 3D cultures were treated with trastuzumab (10 nM), dasatinib (1 μM), or a combination of both drugs. The diameter of the spherical cells (plotted as arbitrary units) after treatment with drugs is shown as means and 95% confidence intervals. Means were compared using the Student *t* test (two-sided). $*P < .001$, trastuzumab vs drug combination; $\#P < .001$, dasatinib vs drug combination.

caused a contraction of these islands, and the contours of the cells were difficult to delineate (Figure 1, D, top panels). We also explored whether the trastuzumab and dasatinib combination affected the three-dimensional growth of BT474 cells. For these experiments, BT474 cells were cultured in Matrigel, a semisolid media in which they form spherical structures. Treatment with the drug combination showed a substantial decrease in the diameter of these spheres, which was not appreciable when cells were treated with the individual agents (trastuzumab vs drug combination, mean diameter = 2.85 vs 1.55 arbitrary units, difference = 1.3 arbitrary units, 95% CI = .96 to 1.63 arbitrary units, $P < .001$; dasatinib vs drug combination, mean diameter = 2.76 vs 1.55 arbitrary units, difference = 1.21 arbitrary units, 95% CI = .82 to 1.59 arbitrary units, $P < .001$) (Figure 1, D, bottom panels, and E).

We also explored whether dasatinib could enhance the action of other drugs used in the therapy of breast cancer. Dasatinib did not substantially increase the antitumoral effect of gemcitabine in BT474 (Supplementary Figure 2, A, available online) and SKBR3 (Supplementary Figure 2, B, available online) cells. However, combination of dasatinib with taxotere or vinorelbine had a higher antitumoral effect than treatment with the individual drugs. Interestingly, addition of trastuzumab to these combinations (dasatinib and gemcitabine, dasatinib and taxotere, dasatinib and vinorelbine) showed augmented antitumoral efficacy.

Coordinated Effects of Trastuzumab and Dasatinib on HER Signaling

To investigate the mechanism responsible for the biological activity of trastuzumab and dasatinib combination, we explored the biochemical changes in both single and combined treatments. Because trastuzumab and dasatinib inhibit tyrosine kinases (8,21), we analyzed their effect on tyrosine phosphorylation in an antibody array containing a panel of 42 different RTKs, including the ones targeted by these drugs. These experiments showed that the most phosphorylated RTKs in BT474 cells corresponded to HER receptors, especially HER2 and HER3 (Figure 2, A). Trastuzumab decreased the level of phosphorylated HER2, but dasatinib had no substantial effect on the amount of phosphorylated HER2. However, trastuzumab and dasatinib combination strongly decreased phosphorylated HER2 and phosphorylated HER3 levels. The drug combination showed analogous results in SKBR3 cells, and both phosphorylated HER2 and phosphorylated HER3 levels were decreased (Supplementary Figure 3, A, available online). Observations were confirmed by immunoprecipitation

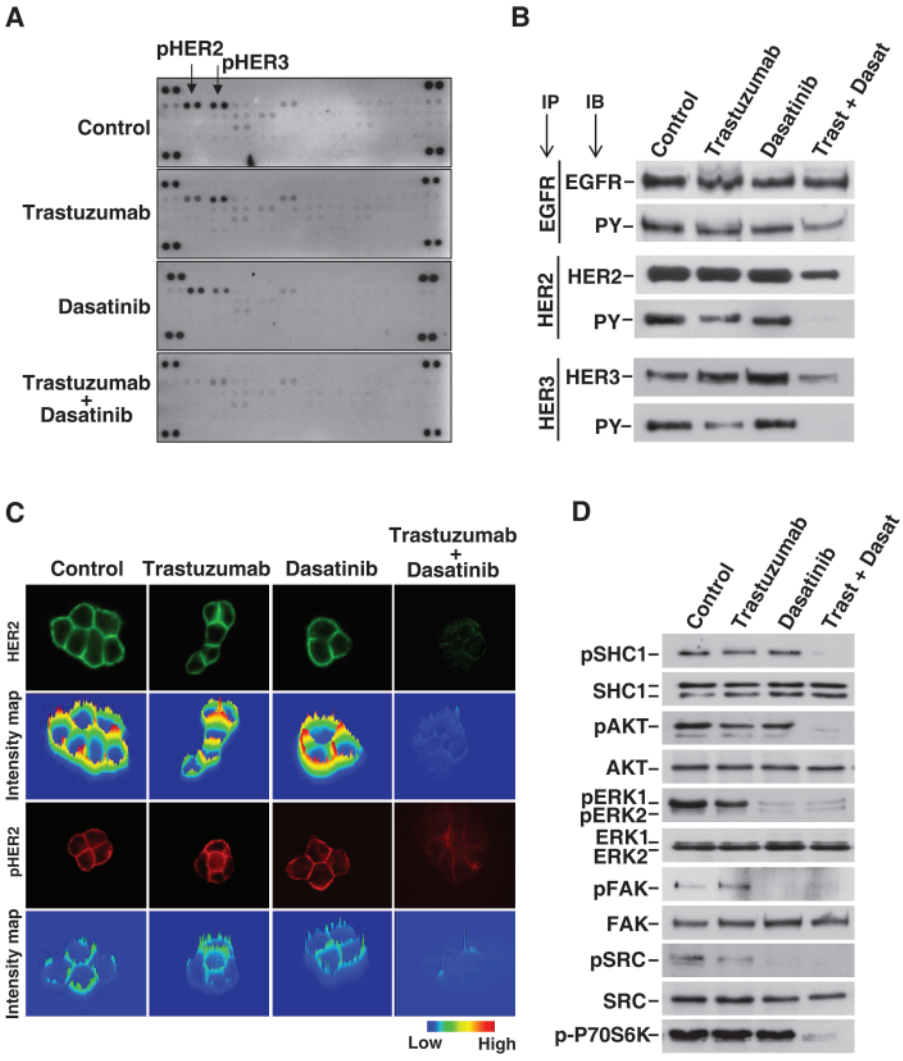

Figure 2. Effect of trastuzumab and dasatinib combination on HER signaling. BT474 cells were treated with the indicated drugs (10 nM trastuzumab, 1 μM dasatinib, or a combination of both drugs) for these experiments. **A**) Cells were treated with drugs for 72 hours, and lysates containing 1 mg protein were analyzed for the level of tyrosine phosphorylation of a panel of 42 receptor tyrosine kinases (RTKs) using the antibody array-based phosphorylation profiling. The levels of phosphorylated HER2 and HER3 are shown (**in the lanes indicated by arrows**). **B)** Analysis of the epidermal growth factor receptor (EGFR) (or HER1), HER2, and HER3 proteins in BT474 cells treated with the respective drugs for 72 hours. Cell lysates were immunoprecipitated (IP) with the anti-EGFR, anti-HER2, and anti-HER3 antibodies, and immunoblots (IB) were performed with the anti-phosphotyrosine antibody (PY). The levels of total HER proteins and the corresponding phosphorylated levels are shown. Total EGFR levels were analyzed and also used as the loading control. **C**) Indirect immunofluorescence microscopy showing the effect of drug combination on the subcellular localization of HER2 and phosphorylated HER2 (pHER2). BT474 cells were seeded on coverslips and treated with the respective drugs for 48 hours. Cell surface expression of HER2 and pHER2 was analyzed with anti-HER2 and anti-pHER2 antibodies and using confocal microscopy. The intensity maps of HER2 and pHER2 were determined using Zeiss LSM 510 software. Reduced HER2 and pHER2 expression was noted after treatment with the drug combination. **D**) Effect of drug treatments on ERK1 and AKT signaling pathways and cytosolic itinerant tyrosine kinases in BT474 cells treated with drugs for 72 hours. Cell lysates were analyzed by immunoblotting for the levels of different proteins, as well as their phosphorylated forms. Total AKT levels were analyzed and also used as the loading control. Dasat = dasatinib; p = phosphorylated; Trast = trastuzumab.

and immunoblotting experiments, and it was also observed that there was a decrease in the total amount of HER2 and HER3 after treatment with the drug combination (Figure 2, B, and Supplementary Figure 3, A, available online). The decrease in HER2 tyrosine phosphorylation induced by the drug combination was also evidenced by immunofluorescence microscopy, and an overall decrease in HER2 on the cell surface was also noted (Figure 2, C). The latter finding was also substantiated by cell surface biotinylation of HER2 proteins (Supplementary Figure 3, B, available online). The combined treatment did not substantially affect the amount of EGFR, although a small decrease in phosphorylated EGFR was detected (Figure 2, B, and Supplementary Figure 3, A, available online).

We reasoned that if the combined treatment with trastuzumab and dasatinib affected tyrosine phosphorylation of HER receptors, the signaling pathways activated by these receptors would consequentially experience an analogous impact. Therefore, we investigated the effect of individual drugs and drug combination on RAS-RAF-MEK-ERK1/2 and phosphatidylinositol 3-kinase–AKT activation pathways, given the important role of these pathways in HER signaling. In addition, we also explored the tyrosine phosphorylation status of the cytosolic itinerant tyrosine kinases c-SRC and FAK, which are well-known dasatinib targets (21). In the resting state of phosphorylation, dasatinib inhibited the dual phosphorylation of ERK1 and tyrosine phosphorylation of c-SRC and FAK (Figure 2, D). The inhibitory effect of trastuzumab and dasatinib combination on phosphorylation was analogous to that of dasatinib, indicating that the activity of combined drugs on these signaling mediators reflect the activity of dasatinib alone. Similar to the effect of the drugs on HER receptors, treatment with the drug combination inhibited the phosphorylation of the adaptor protein SHC1, AKT, as well as a downstream substrate of AKT—the 70 kDa S6 protein kinase (p70S6K). Treatment with individual drugs did not affect the constitutive resting state phosphorylation of these proteins.

Gene Expression Profiling and DNA Damage in Cells Treated With Trastuzumab and Dasatinib

In addition to the biochemical studies, we also performed mRNA expression profiling of BT474 cells treated with trastuzumab, dasatinib, or trastuzumab and dasatinib combination using oligonucleotide arrays. The expression of several genes was altered in response to treatment with the single drugs, but more genes showed altered expression after trastuzumab and dasatinib combination treatment (Figure 3, A). Trastuzumab modified the expression of 181 genes; dasatinib modified the expression of 193 genes; and the drug combination modified the expression of 263 genes. The expression of some genes was modified only by the drug combination and not by individual drugs (Figure 3, A). The drug combination modified the expression of genes involved in cell cycle regulation and DNA recombination and/or repair. Among the most notable cell cycle regulators, whose expression was modified by the drug combination, were CDK2, cyclin E1, cyclin E2, cyclin B1, and p21 (Figure 3, B). The differential expression was statistically significant for all genes shown in the figure ($P < .05$). A time-course analysis of different protein levels demonstrated that the level of p21 decreased within 12 hours, CDK2 and cyclin E1/2 decreased within 36 hours, and cyclin B1 decreased within 24 hours of treatment with the drug combination (Figure 3, C). In contrast, the level of p27, an important negative regulator of cell cycle progression in BT474 cells (30), was substantially increased by the combined treatment of trastuzumab and dasatinib.

Treatment with the drug combination also modified the expression of genes that participate in DNA damage responses (Figure 3, B). This result led us to explore whether treatment with trastuzumab and dasatinib triggered a DNA damage response. Of the many types of DNA damage, the most toxic is DNA DSBs (31,32). The DNA lesions are repaired mainly through nonhomologous end joining or homologous recombination (31). Because RAD51 recombinase, one of the genes whose expression was modified by the combined drug treatment, is involved in homologous recombination, we first investigated whether the drug combination triggered DSBs. Comet assays indicated that treatment of BT474 cells with the drug combination induced the characteristic "comet" appearance of the nuclei, whereas the individual drugs showed no such effect (Figure 3, D).

Upon generation of DSBs, the MRE11A–RAD50–NBS1 (MRN) protein complex is recruited to the sites of the DNA lesions, which triggers the activation of kinases such as ataxia telangiectasia mutated that phosphorylate several downstream mediators (32). One of these downstream molecules is the phosphorylated form of histone H2AX (known as γH2AX), which is used as a surrogate marker for the quantitation of DSBs (33). Immunoblot results showed that γH2AX was detected in cells treated with trastuzumab and dasatinib but not in cells treated with the individual drugs (Figure 3, E). A time-course analysis performed to define the effects of trastuzumab and dasatinib on proteins that participate in the DSB repair pathway verified that the levels of RAD1, RAD51, and RAD54B were substantially decreased by the drug combination (Figure 3, C), and this decrease coincided with the increase in level of γH2AX. The combined drug treatment also increased the level of GADD45γ, which is involved in the DSB repair pathway. The levels of MRE11A and RAD50, both constituents of the MRN complex, were unaffected by trastuzumab and dasatinib combination treatment.

Effect of Trastuzumab and Dasatinib Combination on Apoptosis

The decrease in MTT metabolization in cells treated with dasatinib and trastuzumab could be because of reduced proliferation, cell death, or both. Moreover, the genomic and biochemical studies indicated deregulation of proteins that control these biological processes. Therefore, next we investigated the effect of different drug treatments on cell cycle and apoptosis. In BT474 cells, PI staining revealed a pattern of DNA staining, characterized by a large G0/G1 peak of interphase cells (2n DNA content), a much smaller G2/M peak of cells with duplicated DNA content (4n), and an intermediate subpopulation that corresponded to the S phase (Figure 4, A). Treatment with the individual drugs did not have a substantial effect on the distribution of the different cell cycle phases. However, treatment with the drug combination profoundly affected the PI staining of BT474 cells, which impaired accurate analyses of the action of the drug combination on the different cell cycle phases. We observed that the G0/G1 and

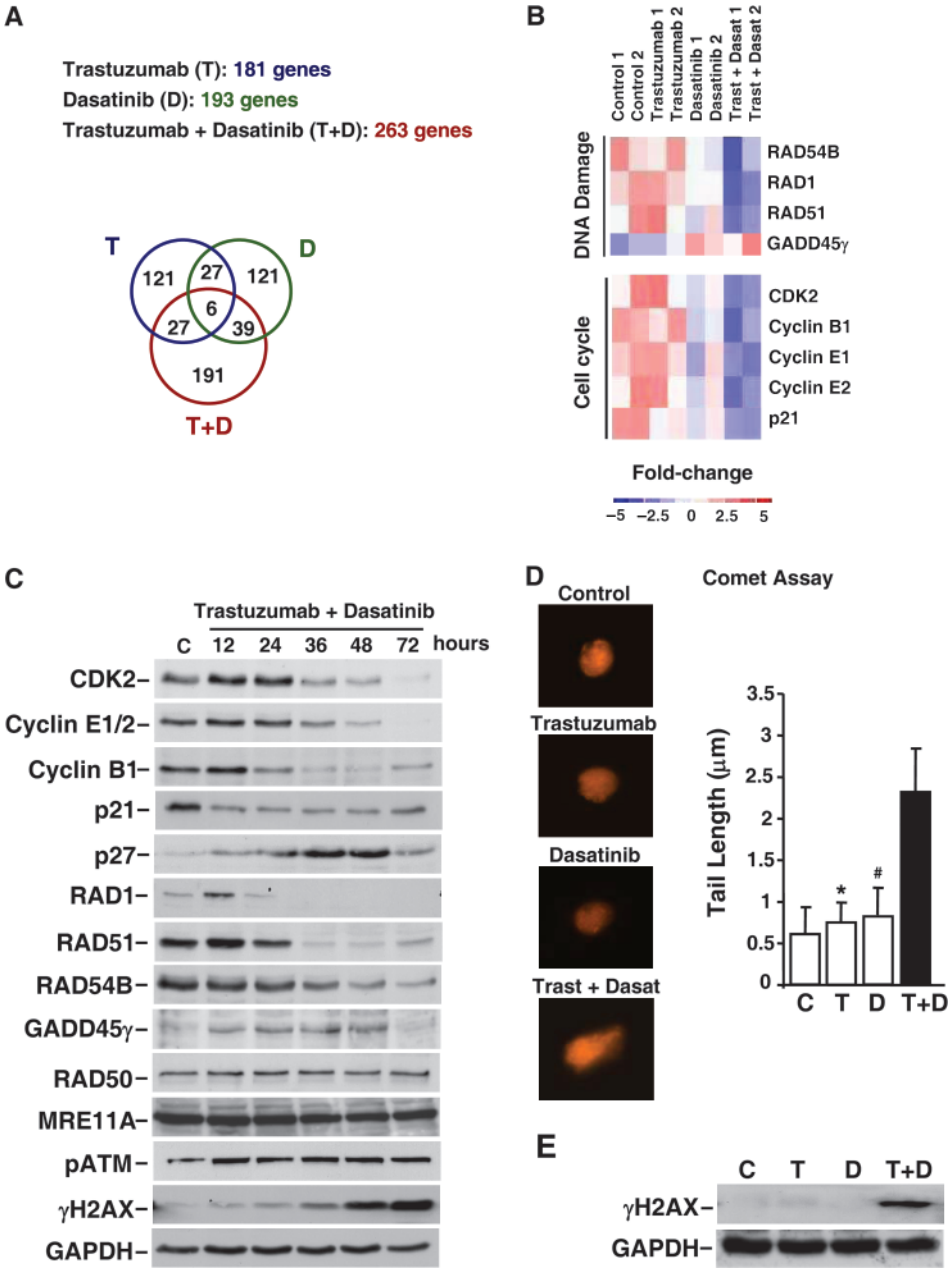

Figure 3. Effect of trastuzumab and dasatinib combination on cell cycle and DNA damage response. BT474 cells were treated with the indicated drugs (10 nM trastuzumab, 1 μM dasatinib, or a combination of both drugs) for these experiments. **A**) Venn diagram depicting the overlap of genes with modified expression levels. **B**) Colorgram of the expression levels of cell cycle and DNA damage genes after 24 hours of treatment with the drugs. Control cells were untreated. **Red**, **white**, and **blue colors** represent the level of gene expression at greater than mean, mean, and lower than mean, respectively. The numeric scale indicates the fold change of expression of each gene in each sample with respect to its mean expression value across all samples. The duplicate samples for each drug or drug combination indicate results from two independent experiments. Trast = trastuzumab. Dasat = dasatinib. **C**) Immunoblot analysis of cells treated with trastuzumab and dasatinib combination for the indicated time in hours. The levels of different proteins involved in cell cycle regulation and DNA damage are shown at different time points. Glyceraldehyde-3-phosphate dehydrogenase was used as the protein loading control. C = control (untreated). **D**) Comet assay of cells treated with different drugs. The images shown are representative of three independent experiments. The tail lengths of the comets are shown in the corresponding bar graph as mean values and 95% confidence intervals. Comparison of means between groups was performed using Student *t* test (two-sided). **P* < .001, trastuzumab vs drug combination; #*P* < .001, dasatinib vs drug combination. C = control (untreated); D = dasatinib; T = trastuzumab; T + D = trastuzumab and dasatinib. **E**) Immunoblot analysis of γH2AX under the conditions described in (**D**).

G2/M peaks decreased in height, and the relative number of cells in the S phase increased. This can be caused by lower sensitivity of S phase cells to the action of the drug combination. An important accumulation of sub-G0 staining was observed in cells treated with the drug combination. As this latter characteristic (ie, accumulation of sub-G0 cells) is indicative of cell death (34), we assessed whether treatment with trastuzumab and dasatinib combination triggered apoptotis in breast cancer cells. Annexin V-fluorescein isothiocyanate staining showed that the number of apoptotic cells was elevated in BT474 cells treated with the drug combination (trastuzumab and

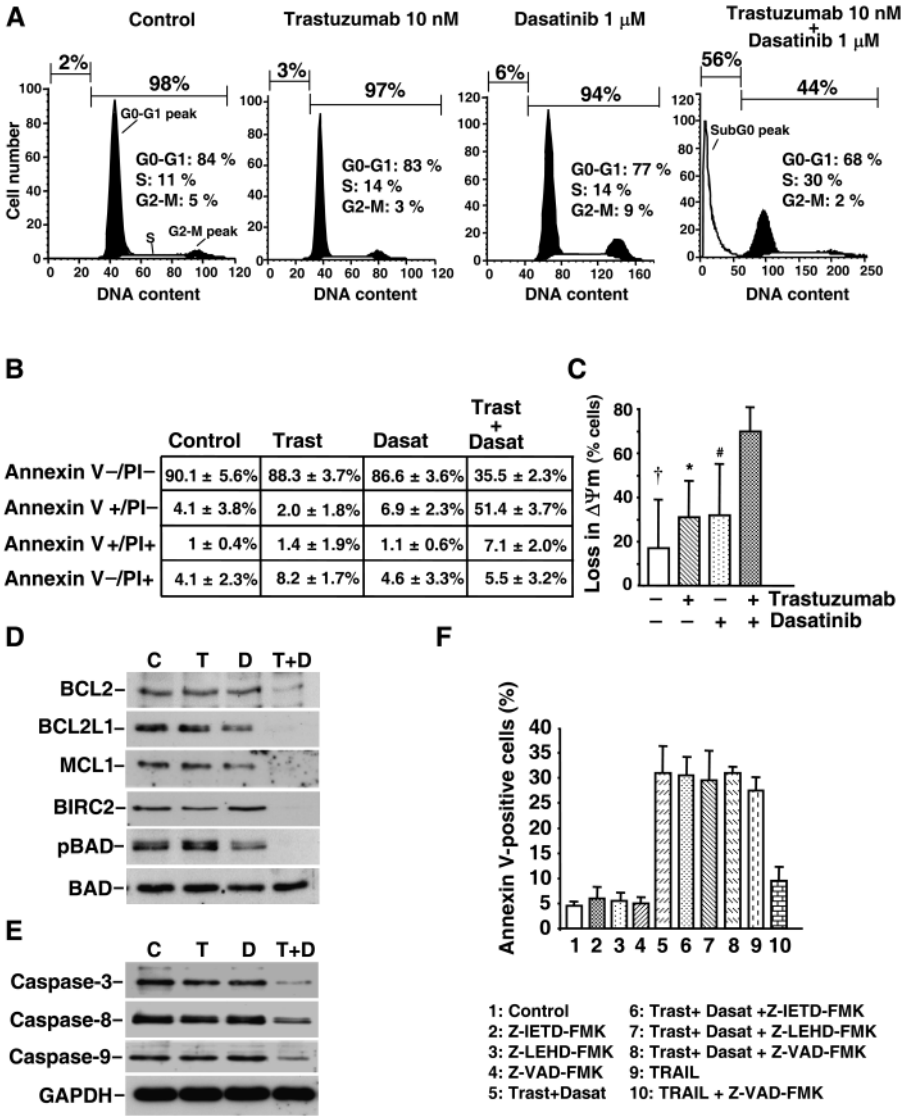

Figure 4. Effect of trastuzumab and dasatinib combination on cell cycle progression and apoptosis. BT474 cells were treated with the indicated drugs (10 nM trastuzumab, 1 μM dasatinib, or a combination of both drugs) for these experiments. **A**) Cells were treated with the indicated drugs for 48 hours, and the cell cycle progression was examined by flow cytometry after staining with propidium iodide (PI). An increase in the sub-G0 peak and decrease in the G0–G1 and G2–M peaks were noted on treatment with the drug combination. The histograms of one representative experiment of the three independent experiments are shown. **B**) Flow cytometry analysis of apoptosis in cells treated with the indicated drugs for 72 hours and stained with Annexin V and PI. The table shows the percentage of cells stained with Annexin V and/or PI. Means and 95% confidence intervals of three independent experiments are shown. Dasat = dasatinib; Trast = trastuzumab. **C**) Cells were treated with the indicated drugs for 48 hours. Flow cytometry analysis of the mitochondrial membrane potential (ΔΨm) was performed after addition of 1 μM tetramethylrhodamine ethyl ester dye. Means and 95% confidence intervals of three independent experiments are shown. Student *t* test (two-sided) was used to compare the mean loss in mitochondrial membrane potential between the groups: †combination vs control, $P = .005$; *combination vs trastuzumab, $P = .019$; #combination vs dasatinib, $P = .032$. **D**) Cells were treated with the indicated drugs for 48 hours, and immunoblot analysis was done for antiapoptotic (BCL2, BCL2L1, BIRC2, MCL1) and proapoptotic (BAD) proteins. C = control (untreated); D = dasatinib; T = trastuzumab. **E**) Immunoblot analysis of caspase-3, -8, and -9 under the same experimental conditions as in (**D**). **F**) Effect of caspase inhibitors on cells treated with the drug combination. Cells were treated with drugs and caspase inhibitors, either individually, or simultaneously, as indicated in the figure. The following concentrations were used: TRAIL (1 nM, combined with 1 μg/mL of cycloheximide to increase the activity of TRAIL), caspase-8 inhibitor (Z-IETD-FMK, 1 μM), caspase 9 inhibitor (Z-LEHD-FMK, 1 μM), and pancaspase inhibitor (Z-VAD-FMK, 1 μM). The cells were stained with Annexin V and analyzed by flow cytometry. The **bar graph** represents the mean percentage of Annexin V-positive cells from three independent experiments. Ninety-five percent confidence intervals are also shown. Control cells were untreated. Dasat = dasatinib; TRAIL = tumor necrosis factor–related apoptosis-inducing ligand; Trast = trastuzumab.

dasatinib combination, 51.4%) compared with cells treated with the individual drugs (trastuzumab, 2%; dasatinib, 6.9%) (Figure 4, B).

Apoptosis may be caused by the loss of membrane potential and increased permeability of the mitochondrial outer membrane (MOM) (35). Analysis of MOM potential indicated that the drug combination affected the membrane potential of a greater number of cells compared with the individual drugs (control vs drug combination, mean loss in MOM potential = 18.67 vs 72.67, difference = 54, 95% CI = 30.04 to 77.95, $P = .005$; trastuzumab vs drug combination, mean loss in MOM potential = 31 vs 72.67, difference = 41.67, 95% CI = 16.53 to 66.79, $P = .019$; dasatinib vs drug combination, mean loss in MOM potential = 31.67 vs 72.67, difference = 41, 95% CI = 8.42 to 73.57, $P = .032$) (Figure 4, C). The results are shown as the percentage of cells that lost TMRE staining. Because the permeability of MOM is regulated by members of the BCL2 family, we analyzed the expression levels of BCL2, BCL2L1, and MCL1 in cells treated with the individual drugs or the combination. The levels of these proteins were not substantially affected after treatment with trastuzumab or dasatinib alone; however, the levels were almost undetectable after treatment with the drug combination. In addition, the levels of phosphorylated BAD (a downstream target of AKT) and BIRC2 also decreased after treatment with the drug combination (Figure 4, D).

To investigate whether a caspase-dependent or independent signaling pathway was involved in apoptosis (36), we assessed the levels of caspase-3, -8, and -9, on treatment with trastuzumab or dasatinib as single drugs, as well as the drug combination (Figure 4, E). Treatment with trastuzumab and dasatinib combination showed a decrease in the level of all three procaspases. It is noteworthy that we were unable to detect the cleaved (active) fragments of these caspases in cells treated with the drug combination. However, when apoptosis was induced in BT474 cells with tumor necrosis factor–related apoptosis-inducing ligand (TRAIL), activation of caspases via generation of cleaved fragments was evident (data not

shown). Furthermore, we used caspase inhibitors to preclude the possibility that caspases were involved in the drug combination–induced apoptosis. Inhibitors of caspase-8 (Z-IETD-FMK), caspase-9 (Z-LEHD-FMK), or a pancaspase inhibitor (Z-VAD-FMK) did not affect the drug combination–induced apoptosis (Figure 4, F). In contrast, the pancaspase inhibitor showed near complete inhibition of TRAIL-induced cell death.

Taken together, these data indicated that although treatment with drug combination decreased the caspase levels, it did not induce their activation, and apoptosis was likely triggered by caspase-independent pathways. One of the caspase-independent pathways that may provoke cell death is caused by release of the apoptosis-inducing factor NAIF1 from the mitochondria (35). NAIF1 is a ubiquitously expressed flavoprotein that is normally localized to the mitochondrial intermembrane space. Increases in MOM permeability caused by apoptotic stimuli cause release of NAIF1 to the cytosol that then moves to the nucleus where it facilitates apoptotic responses, such as nuclear condensation (36). Treatment of BT474 cells with trastuzumab and dasatinib combination showed release of NAIF1 to the cytosolic compartment (Supplementary Figure 3, C, available online).

Efficacy of Trastuzumab and Dasatinib Combination on Tumor Growth In Vivo

To determine whether the synergistic action of the drug combination was also observed in vivo, we implanted BT474 cells into the mammary fat pad of mice randomly assigned to the following four groups—untreated control, dasatinib, trastuzumab, or a combination of trastuzumab and dasatinib. The tumors continued to grow in the untreated group (Figure 5, A), and by day 28 of follow-up, the mice were killed because of the large size of their tumors. In agreement with the in vitro results, the combination of trastuzumab and dasatinib showed a superior antitumoral effect compared with either drug alone (control vs combination, mean volume = 2.6 vs 0.5 cm^3, difference = 2.1 cm^3, 95% CI = 0.76 to 3.51 cm^3, $P = .010$; trastuzumab vs combination, mean tumor volume = 1.5 vs 0.5 cm^3, difference = 1.0 cm^3, 95% CI = 0.12 to 1.93 cm^3, $P = .032$; dasatinib vs combination, mean volume = 1.48 vs 0.5 cm^3, difference 0.98 cm^3, 95% CI = 0.50 to 1.45 cm^3, $P = .003$) (Figure 5, B). It is noteworthy that the tumors from mice treated with the drug combination showed regression, whereas tumors from mice treated with the individual drugs showed stability in size or slight growth (Figure 5, A and B). Because of the strong antitumoral effect of the drug combination, we decided to maintain two mice from this group to follow the evolution of the tumors. In these mice, treatment with trastuzumab and dasatinib combination resulted in complete regression of the tumors by day 36, and the tumors did not relapse at the site of injection even after discontinuation of the treatment for a long period of time (Figure 5, C).

Tumor samples were also analyzed for the phosphorylation levels of HER receptors, as well as the levels of DNA damage response proteins. The combined drug treatment showed a decrease in the level of phosphorylated HER2 compared with control mice or mice treated with the individual drugs (Figure 5, D). The combined drug treatment also showed a decrease in the levels of RAD1, RAD51, RAD54B, and an increase in the level of γH2AX (Figure 5, E).

Discussion

In this study, we showed that the combination of trastuzumab with dasatinib was highly effective against breast cancer cells overexpressing HER2 receptors. Both drugs individually inhibited cell proliferation in vitro and exhibited antitumoral action, but their combination showed a more potent effect on HER2-overexpressing cells. However, compared with single drugs, treatment with the drug combination did not show a greater inhibition of proliferation in cells with normal expression of HER2 receptors. We confirmed these observations in vivo in a mouse mammary fat pad model of breast cancer. Treatment of tumor-bearing mice with the drug combination showed a stronger inhibitory effect on tumor growth than treatment with single drugs. We further demonstrated that there was a complete regression of tumors, even large tumors, in mice treated with the drug combination. In addition, discontinuation of the treatment for 9 months did not result in tumor recurrence.

The mechanistic studies indicated that the drug combination strongly decreased the levels of phosphorylated HER2 and phosphorylated HER3, which were accompanied by a decrease in the total amount of these receptors. We explored whether the combined treatment affected the downstream signaling routes, such as the ERK1 or AKT pathways that regulate cell proliferation and survival (37,38). Dasatinib had the same inhibitory effect on the phosphorylated levels of ERK1 as the combined drug treatment. Therefore, the exclusive inhibition of ERK1 cannot explain the effects of the combined drug treatment on cell proliferation and cell death. Analogously, treatment with dasatinib inhibited SRC or FAK phosphorylation to the same degree as the combined drug treatment. These two kinases are known targets of dasatinib (21) and have been reported to participate in several oncogenic processes (39). We noted that the combined treatment, but not the individual drugs, decreased the level of phosphorylated AKT. Downstream targets of AKT such as p70S6K and BAD were also affected by the combined drug treatment, but not by the individual drugs, as the resting phosphorylated levels of these proteins were reduced on treatment with trastuzumab and dasatinib. The inhibition of different signaling pathways suggests that the synergistic antitumoral action of the combined drug treatment may result from the sum of the inhibition of multiple signaling routes involved in the control of cell proliferation and survival.

Our results showed that the drug combination also affected important regulators of cell cycle progression and a group of proteins involved in DNA repair and/or recombination. Moreover, the drug combination induced DNA DSBs and a DNA damage response that was evidenced by the phosphorylation of H2AX protein. DNA damage can induce cell cycle arrest through activation of kinases such as ataxia telangiectasia mutated (ATM), ataxia telangiectasia and RAD3-related kinase (ATR), and the CHK checkpoint homolog 1 or 2 kinases (CHEK1 or CHEK2, respectively) that reduce CDK activity by various mechanisms (32). The decrease in CDK activity may provoke arrest of cell cycle progression at the G1–S or G2–M checkpoints, which are thought to increase the time available for DNA repair.

The drug combination also induced caspase-independent apoptosis. This was supported by the lack of any effect of the caspase

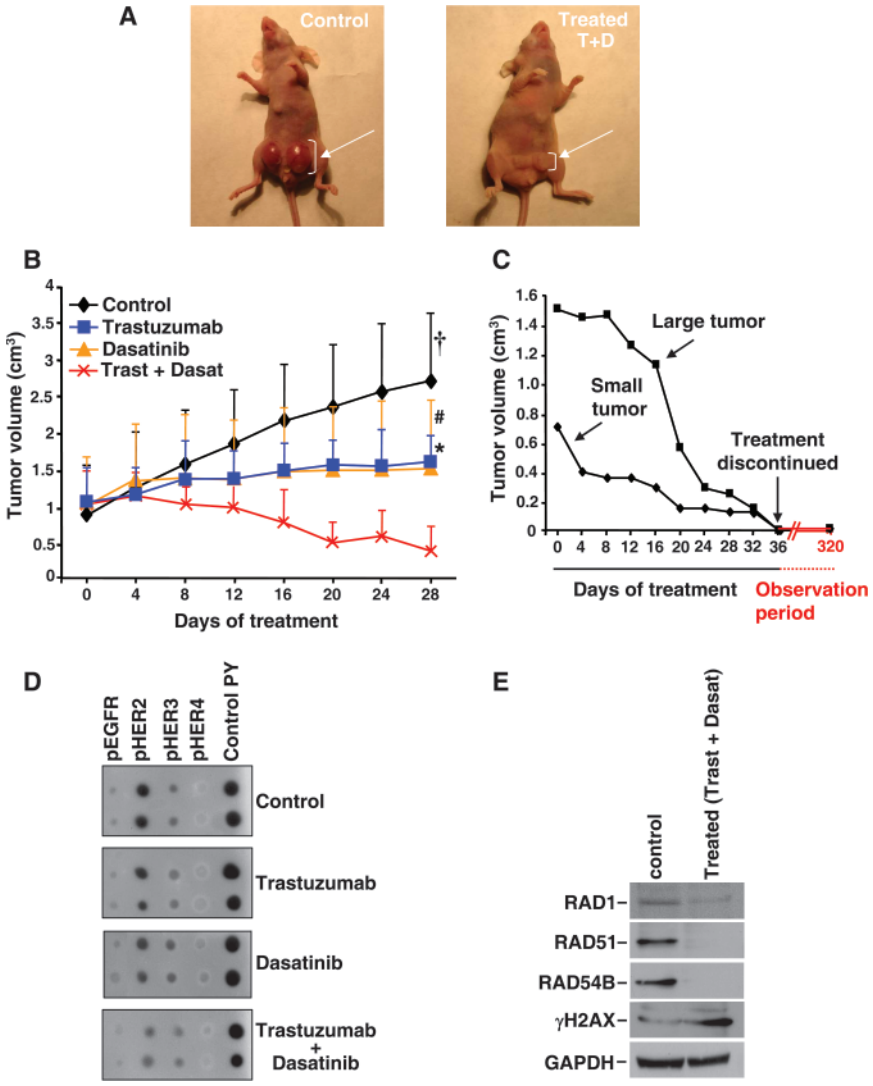

Figure 5. Effect of trastuzumab and dasatinib combination on tumor development in vivo, HER2 phosphorylation, and levels of DNA damage response proteins. **A**) We injected 1 × 10^7 BT474 cells into the mammary fat pad of female BALB/c nude mice. After 2 weeks, mice were either left untreated (control, n = 6) or treated with trastuzumab (T) and dasatinib (D) combination (T + D, n = 6; 600 μg trastuzumab injected abdominally twice a week and once daily orally with 10 mg/kg dasatinib). Tumor growth in representative mouse from control and treated groups on day 28 is shown; the **arrow** indicates the position of the tumor. **B**) Tumor sizes of control mice (n = 6) and those treated with trastuzumab, dasatinib, or the drug combination (n = 6 per group) at the same doses as in (**A**) at the end of the treatment (day 28). Control vs drug combination, †P = .010; trastuzumab vs drug combination, *P = .032; dasatinib vs drug combination, #P = .003. P values were calculated using Student t test (two-sided). **C**) Effect of drug combination on large and small tumors from two mice that showed complete regression of the tumors on day 36 after treatment. The data plotted correspond to the measurements of tumors from two different mice. **D**) Dot blot analysis showing the levels of phosphorylated HER proteins in the tumor xenografts. Control PY = extracts of BT474 cells with high levels of tyrosine-phosphorylated proteins. **E**) Immunoblot analysis of proteins involved in DNA damage response in the tumor xenografts. Tumors from a control mouse and a mouse treated with the drug combination were analyzed. Tumors from two mice for each condition were tested. Representative immunoblot is shown.

inhibitors on apoptosis induced by the drug combination. One of the possible mediators in caspase-independent apoptosis is NAIF1, a protein that is released from the mitochondrial intermembrane space by certain apoptotic stimuli. The release of NAIF1 from the mitochondria to the cytosol, on treatment with the drug combination, indicated that this mechanism could be responsible for caspase-independent apoptosis.

The fact that the drug combination severely affected the DNA repair machinery and led to the accumulation of DSBs raises some questions regarding the mechanism of control of DNA repair machinery by tyrosine kinases and the potential clinical implications. The time-course studies showed a decrease in the level of RAD51 protein, sequentially followed by an accumulation of γH2AX protein. It is possible that the decrease in the level of RAD51 protein impedes adequate repair of spontaneous DNA lesions, and accumulation of such lesions triggers a DNA damage response that results in apoptosis. If that is the case, it is possible that the integrity of the homologous recombination machinery is critically controlled by the interplay of tyrosine kinases sensitive to trastuzumab and dasatinib. In support of our hypothesis, a recent report showed that erlotinib, an inhibitor of EGFR, blocked homologous recombination repair of the DSBs in breast cancer cells through reduction of RAD51 foci formation (40). Previous studies have also indicated that RTKs may regulate DNA repair (41,42). Gefitinib, another EGFR inhibitor, was shown to impede DNA repair in response to ionizing radiations in macrocytic lung cancer cells (41). The mutated forms of MET protein, an RTK implicated in several oncogenic processes such as invasion and metastasis (43) or drug resistance (44), have been reported to bind to and phosphorylate RAD51, facilitating DNA repair in tumor cells (42). Recently, the Williams–Beuren syndrome transcription factor (WSTF; also known as BAZ1B), a tyrosine kinase that is a component of the WICH complex (WSTF-ISWI ATP-dependent chromatin-remodeling complex), has been shown to regulate the DNA damage response through phosphorylation of Tyr142 of H2AX (45).

From the clinical point of view, the fact that trastuzumab and dasatinib combination induced DNA damage in HER2-overexpressing cells in this study, opens up the possibility of combining these drugs in the treatment of HER2-positive breast cancers. In this context, we showed that dasatinib may enhance the activity of treatments for breast cancer that are currently used in the clinics to

treat HER2-positive patients. In addition, our results also offer the interesting option of using dasatinib with other antineoplastic agents in tumors that may be particularly sensitive to DNA damaging drugs or radiotherapy. Interestingly, in head and neck cancer, a radiosensitive tumor, in vitro studies have shown antitumoral activity of agents that target SRC combined with gefitinib (22). Also, the effectiveness of anti-EGFR therapies in colon cancer opens the possibility of exploring whether dasatinib synergizes with anti-HER drugs or radiotherapeutic treatments in these pathologies.

Our study may have a few limitations. Although, the promising findings of this preclinical study indicate potential clinical benefits, we cannot predict the effectiveness or toxicity of the drug combination in humans. Of note, analysis of the antiproliferative effect of the drug combination using the Chou–Talalay algorithm indicated that the lower doses of dasatinib (0.1, 0.25, and 0.5 μM) were additive to trastuzumab, whereas the dose of 1 μM showed synergistic effect. The latter is an achievable concentration (20), but the fact that the synergistic effect was observed at a high concentration of dasatinib should be taken into account for the adequate design of clinical trials.

References

1. Blume-Jensen P, Hunter T. Oncogenic kinase signalling. *Nature.* 2001; 411(6835):355–365.
2. Hynes NE, Lane HA. ERBB receptors and cancer: the complexity of targeted inhibitors. *Nat Rev Cancer.* 2005;5(5):341–354.
3. Slamon DJ, Clark GM, Wong SG, Levin WJ, Ullrich A, McGuire WL. Human breast cancer: correlation of relapse and survival with amplification of the HER-2/neu oncogene. *Science.* 1987;235(4785):177–182.
4. Di Fiore PP, Pierce JH, Kraus MH, Segatto O, King CR, Aaronson SA. *erb*B-2 is a potent oncogene when overexpressed in NIH/3T3 cells. *Science.* 1987;237(4811):178–182.
5. Muthuswamy SK, Li D, Lelievre S, Bissell MJ, Brugge JS. ErbB2, but not ErbB1, reinitiates proliferation and induces luminal repopulation in epithelial acini. *Nat Cell Biol.* 2001;3(9):785–792.
6. Moody SE, Sarkisian CJ, Hahn KT, et al. Conditional activation of Neu in the mammary epithelium of transgenic mice results in reversible pulmonary metastasis. *Cancer Cell.* 2002;2(6):451–461.
7. Moody SE, Perez D, Pan TC, et al. The transcriptional repressor Snail promotes mammary tumor recurrence. *Cancer Cell.* 2005;8(3):197–209.
8. Nahta R, Esteva FJ. Trastuzumab: triumphs and tribulations. *Oncogene.* 2007;26(25):3637–3643.
9. Yarden Y, Sliwkowski MX. Untangling the ErbB signalling network. *Nat Rev Mol Cell Biol.* 2001;2(2):127–137.
10. Slamon DJ, Leyland-Jones B, Shak S, et al. Use of chemotherapy plus a monoclonal antibody against HER2 for metastatic breast cancer that overexpresses HER2. *N Engl J Med.* 2001;344(11):783–792.
11. Baselga J, Perez EA, Pienkowski T, Bell R. Adjuvant trastuzumab: a milestone in the treatment of HER-2-positive early breast cancer. *Oncologist.* 2006;11(suppl 1):4–12.
12. Ocana A, Pandiella A. Identifying breast cancer druggable oncogenic alterations: lessons learned and future targeted options. *Clin Cancer Res.* 2008;14(4):961–970.
13. Nahta R, Yu D, Hung MC, Hortobagyi GN, Esteva FJ. Mechanisms of disease: understanding resistance to HER2-targeted therapy in human breast cancer. *Nat Clin Pract Oncol.* 2006;3(5):269–280.
14. Esparis-Ogando A, Ocana A, Rodriguez-Barrueco R, Ferreira L, Borges J, Pandiella A. Synergic antitumoral effect of an IGF-IR inhibitor and trastuzumab on HER2-overexpressing breast cancer cells. *Ann Oncol.* 2008;19(11):1860–1869.
15. Nielsen TO, Hsu FD, Jensen K, et al. Immunohistochemical and clinical characterization of the basal-like subtype of invasive breast carcinoma. *Clin Cancer Res.* 2004;10(16):5367–5374.
16. Finn RS. Targeting Src in breast cancer. *Ann Oncol.* 2008;19(8): 1379–1386.
17. Finn RS, Dering J, Ginther C, et al. Dasatinib, an orally active small molecule inhibitor of both the src and abl kinases, selectively inhibits growth of basal-type/"triple-negative" breast cancer cell lines growing in vitro. *Breast Cancer Res Treat.* 2007;105(3):319–326.
18. van Agthoven T, Sieuwerts AM, Meijer-van Gelder ME, et al. Relevance of breast cancer antiestrogen resistance genes in human breast cancer progression and tamoxifen resistance. *J Clin Oncol.* 2009;27(4):542–549.
19. Rix U, Hantschel O, Durnberger G, et al. Chemical proteomic profiles of the BCR-ABL inhibitors imatinib, nilotinib, and dasatinib reveal novel kinase and nonkinase targets. *Blood.* 2007;110(12):4055–4063.
20. Huang F, Reeves K, Han X, et al. Identification of candidate molecular markers predicting sensitivity in solid tumors to dasatinib: rationale for patient selection. *Cancer Res.* 2007;67(5):2226–2238.
21. Karaman MW, Herrgard S, Treiber DK, et al. A quantitative analysis of kinase inhibitor selectivity. *Nat Biotechnol.* 2008;26(1):127–132.
22. Koppikar P, Choi SH, Egloff AM, et al. Combined inhibition of c-Src and epidermal growth factor receptor abrogates growth and invasion of head and neck squamous cell carcinoma. *Clin Cancer Res.* 2008;14(13):4284–4291.
23. Esparis-Ogando A, Diaz-Rodriguez E, Montero JC, Yuste L, Crespo P, Pandiella A. Erk5 participates in neuregulin signal transduction and is constitutively active in breast cancer cells overexpressing ErbB2. *Mol Cell Biol.* 2002;22(1):270–285.
24. Agus DB, Akita RW, Fox WD, et al. Targeting ligand-activated ErbB2 signaling inhibits breast and prostate tumor growth. *Cancer Cell.* 2002; 2(2):127–137.
25. Cabrera N, Diaz-Rodriguez E, Becker E, Martin-Zanca D, Pandiella A. TrkA receptor ectodomain cleavage generates a tyrosine-phosphorylated cell-associated fragment. *J Cell Biol.* 1996;132(3):427–436.
26. Esparis-Ogando A, Diaz-Rodriguez E, Pandiella A. Signalling-competent truncated forms of ErbB2 in breast cancer cells: differential regulation by protein kinase C and phosphatidylinositol 3-kinase. *Biochem J.* 1999; 344(pt 2):339–348.
27. Chou TC, Talalay P. Quantitative analysis of dose-effect relationships: the combined effects of multiple drugs or enzyme inhibitors. *Adv Enzyme Regul.* 1984;22:27–55.
28. Li C, Wong WH. Model-based analysis of oligonucleotide arrays: expression index computation and outlier detection. *Proc Natl Acad Sci U S A.* 2001;98(1):31–36.
29. Gallo V, Khan A, Gonzales C, et al. Validation of biomarkers for the study of environmental carcinogens: a review. *Biomarkers.* 2008;13(5):505–534.
30. Lane HA, Beuvink I, Motoyama AB, Daly JM, Neve RM, Hynes NE. ErbB2 potentiates breast tumor proliferation through modulation of p27(Kip1)-Cdk2 complex formation: receptor overexpression does not determine growth dependency. *Mol Cell Biol.* 2000;20(9):3210–3223.
31. Jackson SP, Bartek J. The DNA-damage response in human biology and disease. *Nature.* 2009;461(7267):1071–1078.
32. Harper JW, Elledge SJ. The DNA damage response: ten years after. *Mol Cell.* 2007;28(5):739–745.
33. Burma S, Chen BP, Murphy M, Kurimasa A, Chen DJ. ATM phosphorylates histone H2AX in response to DNA double-strand breaks. *J Biol Chem.* 2001;276(45):42462–42467.
34. Galluzzi L, Aaronson SA, Abrams J, et al. Guidelines for the use and interpretation of assays for monitoring cell death in higher eukaryotes. *Cell Death Differ.* 2009;16(8):1093–1107.
35. Danial NN, Korsmeyer SJ. Cell death: critical control points. *Cell.* 2004; 116(2):205–219.
36. Tait SW, Green DR. Caspase-independent cell death: leaving the set without the final cut. *Oncogene.* 2008;27(50):6452–6461.
37. Garcia-Echeverria C, Sellers WR. Drug discovery approaches targeting the PI3K/Akt pathway in cancer. *Oncogene.* 2008;27(41):5511–5526.
38. Roberts PJ, Der CJ. Targeting the Raf-MEK-ERK mitogen-activated protein kinase cascade for the treatment of cancer. *Oncogene.* 2007;26(22): 3291–3310.
39. Kim LC, Song L, Haura EB. Src kinases as therapeutic targets for cancer. *Nat Rev Clin Oncol.* 2009;6(10):587–595.
40. Li L, Wang H, Yang ES, Arteaga CL, Xia F. Erlotinib attenuates homologous recombinational repair of chromosomal breaks in human breast cancer cells. *Cancer Res.* 2008;68(22):9141–9146.

41. Tanaka T, Munshi A, Brooks C, Liu J, Hobbs ML, Meyn RE. Gefitinib radiosensitizes non-small cell lung cancer cells by suppressing cellular DNA repair capacity. *Clin Cancer Res.* 2008;14(4):1266–1273.
42. Ganapathipillai SS, Medova M, Aebersold DM, et al. Coupling of mutated Met variants to DNA repair via Abl and Rad51. *Cancer Res.* 2008;68(14): 5769–5777.
43. Benvenuti S, Comoglio PM. The MET receptor tyrosine kinase in invasion and metastasis. *J Cell Physiol.* 2007;213(2):316–325.
44. Engelman JA, Zejnullahu K, Mitsudomi T, et al. MET amplification leads to gefitinib resistance in lung cancer by activating ERBB3 signaling. *Science.* 2007;316(5827):1039–1043.
45. Xiao A, Li H, Shechter D, et al. WSTF regulates the H2A.X DNA damage response via a novel tyrosine kinase activity. *Nature.* 2009; 457(7225):57–62.

Funding

Ministry of Science and Innovation of Spain (BFU2006-01813/BMC-FEDER), the Instituto de Salud Carlos III through the Spanish Cancer Centers Network Program (RD06/0020/0041), and an Acción transversal en cancer to A.P. S.S. and J.C.M. were supported by Juan de la Cierva and Scientific Foundation of the Spanish Association Against Cancer (AECC) contracts, respectively. This work was partially sponsored by a research contract to AP from Bristol-Myers Squibb, S.A., Madrid, Spain.

Notes

The sponsors did not have any role in the study design, collection of data, interpretation of the results, preparation of the article, or the decision to submit the article for publication.

The authors thank Dr Azucena Esparís-Ogando for her critical comments on the manuscript.

Affiliations of authors: Instituto de Biología Molecular y Celular del Cáncer, CSIC-Universidad de Salamanca, Salamanca, Spain (SS, JCM, AP); Servicio de Oncología Médica, Complejo Hospitalario Universitario de Albacete, AECC Unit, Albacete, Spain (AO).